

Metabolic Architecture of the Cereal Grain and Its Relevance to Maximize Carbon Use Efficiency¹[OPEN]

Hardy Rolletschek², Eva Grafahrend-Belau², Eberhard Munz, Volodymyr Radchuk, Ralf Kartäusch, Henning Tschiersch, Gerd Melkus, Falk Schreiber, Peter M. Jakob, and Ljudmilla Borisjuk*

Department of Molecular Genetics, Leibniz Institute of Plant Genetics and Crop Plant Research, 06466 Gatersleben, Germany (H.R., E.M., V.R., H.T., L.B.); Institut für Pharmazie, Martin-Luther-University of Halle, 06120 Halle, Germany (E.G.-B.); Institute of Experimental Physics 5, University of Würzburg, 97074 Würzburg, Germany (E.M., P.M.J.); Research Center Magnetic Resonance Bavaria, 97074 Würzburg, Germany (R.K., P.M.J.); Department of Medical Imaging, University of Ottawa, Ottawa, Ontario, Canada K1Y 4E9 (G.M.); and Clayton School of IT, Monash University, Melbourne, Victoria 3800, Australia (F.S.)

ORCID IDs: 0000-0002-8619-1391 (H.R.); 0000-0002-4994-3304 (E.M.); 0000-0001-5387-8958 (G.M.); 0000-0002-3481-5545 (P.M.J.); 0000-0001-6910-0841 (L.B.).

Here, we have characterized the spatial heterogeneity of the cereal grain's metabolism and demonstrated how, by integrating a distinct set of metabolic strategies, the grain has evolved to become an almost perfect entity for carbon storage. In vivo imaging revealed light-induced cycles in assimilate supply toward the ear/grain of barley (*Hordeum vulgare*) and wheat (*Triticum aestivum*). In silico modeling predicted that, in the two grain storage organs (the endosperm and embryo), the light-induced shift in solute influx does cause adjustment in metabolic flux without changes in pathway utilization patterns. The enveloping, leaf-like pericarp, in contrast, shows major shifts in flux distribution (starch metabolism, photosynthesis, remobilization, and tricarboxylic acid cycle activity) allow to refix 79% of the CO₂ released by the endosperm and embryo, allowing the grain to achieve an extraordinary high carbon conversion efficiency of 95%. Shading experiments demonstrated that ears are autonomously able to raise the influx of solutes in response to light, but with little effect on the steady-state levels of metabolites or transcripts or on the pattern of sugar distribution within the grain. The finding suggests the presence of a mechanism(s) able to ensure metabolic homeostasis in the face of short-term environmental fluctuation. The proposed multicomponent modeling approach is informative for predicting the metabolic effects of either an altered level of incident light or a momentary change in the supply of sucrose. It is therefore of potential value for assessing the impact of either breeding and/or biotechnological interventions aimed at increasing grain yield.

Raising the productivity of a given crop genotype requires an increase in the plant's ability to efficiently respond to a changeable environment. At the physiological level, this involves adjustments to the photosynthetic activity of its leaves, to the control of assimilate movement from source to sink, and to the

efficiency of assimilate storage. The manipulation of the plant's efficiency to fix carbon, to use energy and nutrients, and to utilize water has been suggested as a route for improving crop productivity (Amthor 2010; De Block and Van Lijsebettens, 2011). Particular attention has been devoted to the cereals, given their central role in the human diet. While the necessary integration of physiological and developmental processes in all plants relies on the transmission of hormonal, metabolic, and other signals through the vascular system (van Bel et al., 2013), this is not the case in the cereal grain, because this network does not extend beyond the pericarp, a maternal structure that encloses the filial storage organs (embryo and endosperm; Radchuk and Borisjuk, 2014). The isolation of the filial from the maternal tissues in the cereal grain creates a complex metabolic system, involving, at the least, a tripartite interaction between the pericarp, endosperm, and embryo. These three grain components in effect form an interactive system of autonomous organs, each following their own genetic programs (Sreenivasulu et al., 2006). The idea that the cereal grain is a metabolically homogeneous unit is an oversimplification, even if it is a useful assumption for metabolism and growth

¹ This work was supported by the German Plant Phenotyping Network.

² These authors contributed equally to the article.

* Address correspondence to borysyuk@ipk-gatersleben.de.

The author responsible for distribution of materials integral to the findings presented in this article in accordance with the policy described in the Instructions for Authors (www.plantphysiol.org) is: Ljudmilla Borisjuk (borysyuk@ipk-gatersleben.de).

H.R. and L.B. designed the research, performed the research (metabolite analysis and histology), analyzed the data, and wrote the article; E.G.-B. performed the flux balance analysis research, interpreted the data, and wrote the article; E.M., G.M., and R.K. performed the research (NMR/magnetic resonance imaging) and analyzed the data; V.R. performed the research (transcriptomics); H.T. performed the research (photosynthesis and gas exchange); and F.S. and P.M.J. analyzed the data.

[OPEN] Articles can be viewed without a subscription.

www.plantphysiol.org/cgi/doi/10.1104/pp.15.00981

modeling (Grafahrend-Belau et al., 2013). There is a growing requirement to specify whole-grain metabolism at the level of its component tissue parts.

Given that metabolic activity varies qualitatively from tissue to tissue within the plant, approaches that can deliver a high level of spatial resolution are needed to gain a holistic picture of metabolism. Toward this end, various approaches have been successfully applied, e.g. mass spectrometry imaging (Peukert et al., 2014) and laser microdissection-coupled analytics (Schiebold et al., 2011; Belmonte et al., 2013). While such approaches can provide an excellent level of static chemical and/or spatial resolution, it is invasive and thus has only limited ability to generate dynamic measurements. A number of noninvasive imaging platforms, capable of monitoring growth and metabolism at different levels of spatial resolution, have been developed in recent years. The three leading ones are NMR, magnetic resonance imaging (MRI), and positron emission tomography, all of which have been used to characterize sap flow in live material (Köckenberger et al., 2004; Van As and van Duynhoven, 2013). The small size and complex structure of some seeds (and even of the cereal grain) present a technical challenge in applying such technologies (Borisjuk et al., 2012).

A further challenge relates to the temporal variability in grain metabolism induced by environmental fluctuations. The supply of assimilate to the developing ear and grain is assumed to underlay significant diurnal variations (Grafahrend-Belau et al., 2013; Cheung et al., 2014), but their experimental validation has remained difficult to achieve. Diurnal variation in transcript abundance in barley (*Hordeum vulgare*) grains has been found (Mangelsen et al., 2010), but it is unclear whether transcriptomic changes are mirrored by (proportional) changes to the metabolic activity. Where experimentation is difficult, it may be possible to exploit in silico metabolic modeling, an approach that has been validated in the form of flux balance analysis (FBA; Sweetlove and Ratcliffe, 2011; Baghalian et al., 2014). FBA represents an established technique to generate quantitative models of optimal steady-state flux distributions at large-scale metabolic networks. Appropriate FBA models involving seed metabolism (Grafahrend-Belau et al., 2009; Hay and Schwender, 2011; Hay et al., 2014) and even individual seed organs/tissues (Rolletschek et al., 2011; Borisjuk et al., 2013) have been elaborated. As yet, however, these seed models cannot account for the exchange of materials between the individual tissues/organs. The challenge now is to join up specific models to form a multilayered representation of entire tissues/organs/organisms (Mintz-Oron et al., 2012; Grafahrend-Belau et al., 2013; Gomes de Oliveira Dal'Molin et al., 2015). Such an approach could represent a useful means of identifying the key drivers of metabolic behavior and the major bottlenecks, which could then be viewed as viable targets for intervention (Sweetlove et al., 2014).

The aim of this research was to gain a picture of the metabolic architecture of the cereal grain, in particular

to recognize the separate contribution made to the grain's metabolism by each of the three grain components (embryo, endosperm, and pericarp) and to explore how they respond to fluctuating environments (light/Suc supply). By applying noninvasive NMR/MRI technology, we first monitored temporal variability in solute flow toward the living ear/grain and could detect significant light-dependent (diurnal) cycles. Based on the experimental quantification of biomass composition, growth rate, metabolite abundance, gas exchange, and photosynthetic activity, we then generated component-specific stoichiometric models that were eventually combined into a multicomponent grain model, accounting for the exchange of materials between the grain organs. We predicted component-specific metabolic fluxes under light (day) versus dark (night) conditions and performed shading experiments with subsequent analysis of assimilate uptake/partitioning and metabolite/transcript abundance, allowing to illuminate the dynamic aspects of grain metabolism under fluctuating environmental conditions. Overall, our work provides a unique framework for metabolic modeling and perspectives for understanding the control of cereal grain metabolism.

RESULTS

Monitoring the Sap Flow to the Individual Ear Using NMR Demonstrates Fast Light Responses and Indicates Ear-Autonomous Regulatory Mechanisms

In an attempt to determine whether sap flow toward the cereal ear responded to illumination in vivo, we used unique NMR technology (alternating current [AC]-gradient method for velocity profile measurement; Kartäusch et al., 2014). The AC-gradient method is feasible for fast and noninvasive in vivo detection of low fluxes under high endogenous water background. An additional advantage is that the low-field NMR instrument is transportable and allows for monitoring plants in their natural environment. The NMR coil was attached to the base of a wheat (*Triticum aestivum*) ear (peduncle) to monitor solute flux during several days. Peduncle is the only way for sap flow toward the ear and thus is appropriate to determine the direction of net flux and quantify its velocity. The plant was exposed to a 12-h photoperiod (corresponding to the yellow and white areas shown in Fig. 1A). The resulting NMR output revealed that the flux responded to illumination by a 3- to 4-fold change. Similarly, the switch to darkness resulted in an instant decrease in the flux, an effect that was reproducible over several days. A similar outcome was observed when the same setup was applied to a barley plant (Fig. 1B). This in vivo experiment indicates the existence of significant diurnal cycles in assimilate supply toward the growing ear/grain, probably induced by the photoperiod experienced by the plant.

In the same experiment, an individual ear was kept in the dark at the same time that the rest of the plant remained exposed to a diurnal variation in light. This is

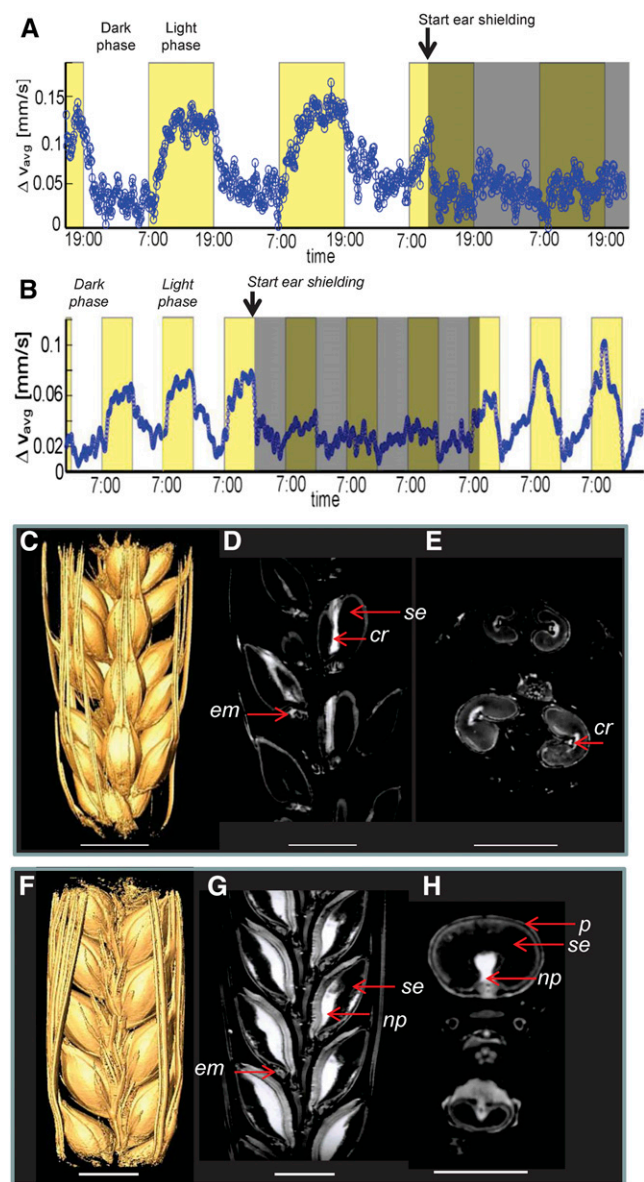


Figure 1. NMR-based in vivo analysis of solute flux toward the ear of wheat/barley and structural modeling. A and B, Monitoring of the solute flux average (ΔV_{avg}) of a wheat (A) and barley (B) plant exposed to a 12-h photoperiod. The gray region indicates shielding of the ear above the NMR coil while the remainder of the plant still experienced the light/dark cycle. C to H, Ear modeling in wheat (C–E) and barley (F–H). The three-dimensional ear models (C and F) were derived from MRI data and are shown in more detail as Supplemental Movies S1 and S2. D and G, Longitudinal sections. E and H, Transverse sections. See also Supplemental Movies S3 and S4. *cr*, Crease; *em*, embryo; *np*, nucellar projection; *p*, pericarp; *se*, starchy endosperm. Bars = 5 mm.

referred to henceforth as ear shielding. In this case, the light response of the ear was abolished, and the flux remained at the low level characteristic of nonlit conditions (Fig. 1, A and B). Once the ear shielding was removed, the light response recovered fully after 3 to 4 d. The conclusion was that both the wheat and barley

ear are able to quickly and autonomously regulate sap flow in response to ambient light conditions.

MRI Indicates Localized Changes in Grain's Transport Route

Noninvasive MRI was used to visualize light responses of individual grains. The ear houses numerous grains, all at slightly different stages of development, and so all follow their own metabolic program. Three-dimensional MRI-based models of the central part of an intact wheat (barley) ear are shown in Figure 1, C and F, and Supplemental Movies S1 and S2. MRI could display the internal structure of a number of grains with a spatial resolution ($104 \times 208 \times 208$ mm) sufficient to enable the recognition of the pericarp, endosperm, and embryo (Fig. 1, D, E, and G, ^1H ; Supplemental Movies S3 and S4). An intense ^1H -NMR signal (signifying high water content) was observed in the crease region and especially in the nucellar projection and the endosperm (apoplastic) cavity. The light response of individual wheat grains was monitored via MRI, tracking a number of grains over an 18-h period (6 h of dark, 6 h of light, and 6 h of dark). The T2 value, which reflects a combination of water content and cell size in living tissue (Van der Weerd et al., 2002; Van As, 2007), rose statistically significantly in response to illumination (Student's *t* test, $P < 0.05$; Fig. 2A), implying an increase in the water content/cell size of the grain (Krishnan et al., 2004, 2014). Image analysis revealed that changes in T2 were confined to small regions of the wheat grains (from 0.63 to 0.78 mm 3 ; Fig. 2B), colocalizing with the crease (Fig. 2, C–E). Tissues within this region are known to be responsible for solute transfer into the grain (Fisher and Cash-Clark, 2000; Andriunas et al., 2013) and are structurally arranged to facilitate the flow and release of solute into the endosperm (Melkus et al., 2011; Radchuk and Borisjuk, 2014). The implication is that individual grains responded to illumination by increasing the influx of water/solutes, evident by local changes of tissue parameters along the main transport route.

Defining the Metabolic Heterogeneity of the Grain as the Basis for a Modeling Approach

An FBA-based metabolic modeling approach was applied to get insight into the metabolic responses of light-stimulated assimilate uptake in the developing barley grain. The in silico study was based on a multi-component grain model to take into account that the grain represents a nonhomogeneous metabolic system comprising the pericarp, the endosperm, and the embryo, each endowed with its distinct metabolic features. A structural overview on the developing grain (approximately 20 d after fertilization [DAF]) is given in Figure 3A. The vein is embedded in the pericarp and provides assimilates/water to the central endosperm region via the nucellar projection (Fig. 3B). The endosperm specializes in starch accumulation (Fig. 3D; Rolletschek et al., 2004), and the embryo accumulates a

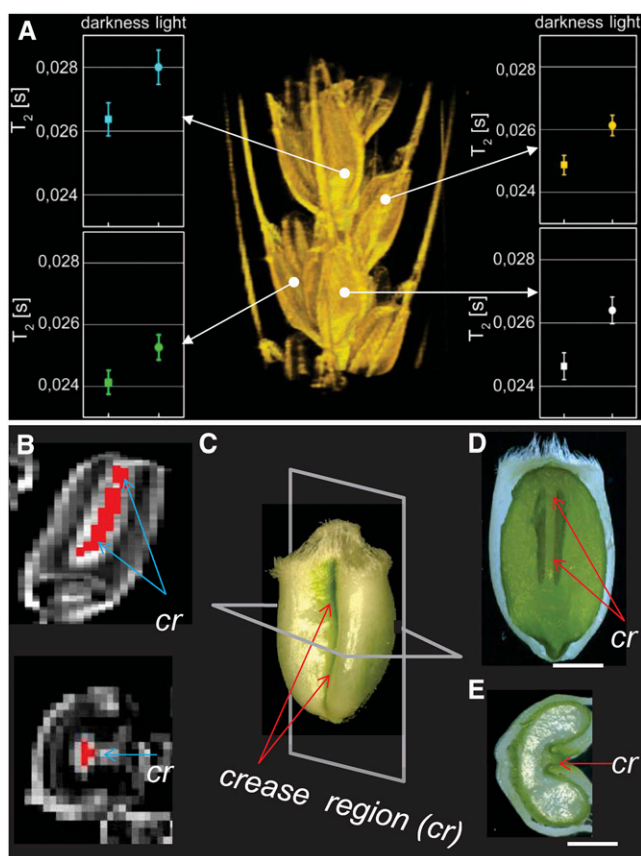


Figure 2. In vivo analysis of light responses in developing wheat grains based on MRI. A, T₂ times measured for four individual grains of an intact wheat ear under dark versus light conditions. Mean values \pm SD are presented. B, Localization of the responsive region in grain (fragments of three-dimensional data sets are shown where T₂ value significantly changed): colored region in longitudinal (above) and cross section (below). C to E, Light microscopic image of grain (C) showing the corresponding section level in (D and E). cr, Crease. Bars = 1 mm.

mixture of lipids and proteins (Fig. 3E; Neuberger et al., 2008). Some lipids also accumulate in the aleurone layer of the peripheral endosperm. The pericarp is photosynthetically active (Fig. 3F; Tschiersch et al., 2011), contributes to the alleviation of the hypoxic conditions prevailing within the central endosperm (Rolletschek et al., 2011), and mediates the delivery of assimilate into the embryo and endosperm (Melkus et al., 2011).

Generation and Parameterization of the Multicomponent FBA Grain Model

As the first step, component-specific stoichiometric models for metabolism had to be constructed, based on a combination of literature-based biochemical, physiological, proteomic, and genomic data and our own unpublished experimental data. The second step combined the three individual models into a multicomponent grain model in which the pericarp mediated the transport of O₂, CO₂, C, N, and SO₄²⁻ between the other components,

thereby providing the link between the maternal and filial metabolism (Fig. 3). Compound exchange between the embryo and endosperm was not considered given the lack of any experimental evidence for this process. The resulting network included 906 metabolites, 716 biochemical reactions, and 201 translocation processes.

To parameterize the FBA model, it was necessary to experimentally quantify the biomass composition and growth rates of each component (pericarp, endosperm, and embryo), the gas (O₂ and CO₂) exchange rate of the grain as a whole, the volume of each component, and the pericarp's electron transport rate (all data are given in Supplemental Data Set S1). The focus was on the barley grains 18 to 22 DAF, a developmental stage during which both the endosperm and embryo are experiencing a rapid growth in biomass, while the biomass of the pericarp remains unchanged (Radchuk et al., 2011).

The multicomponent model was analyzed using FBA with an objective function to minimize the uptake of carbon sources per flux unit within the specified constraints. Flux ranges were calculated using flux variability analysis. The predicted fluxes were considered to significantly differ between conditions if their flux ranges did not overlap.

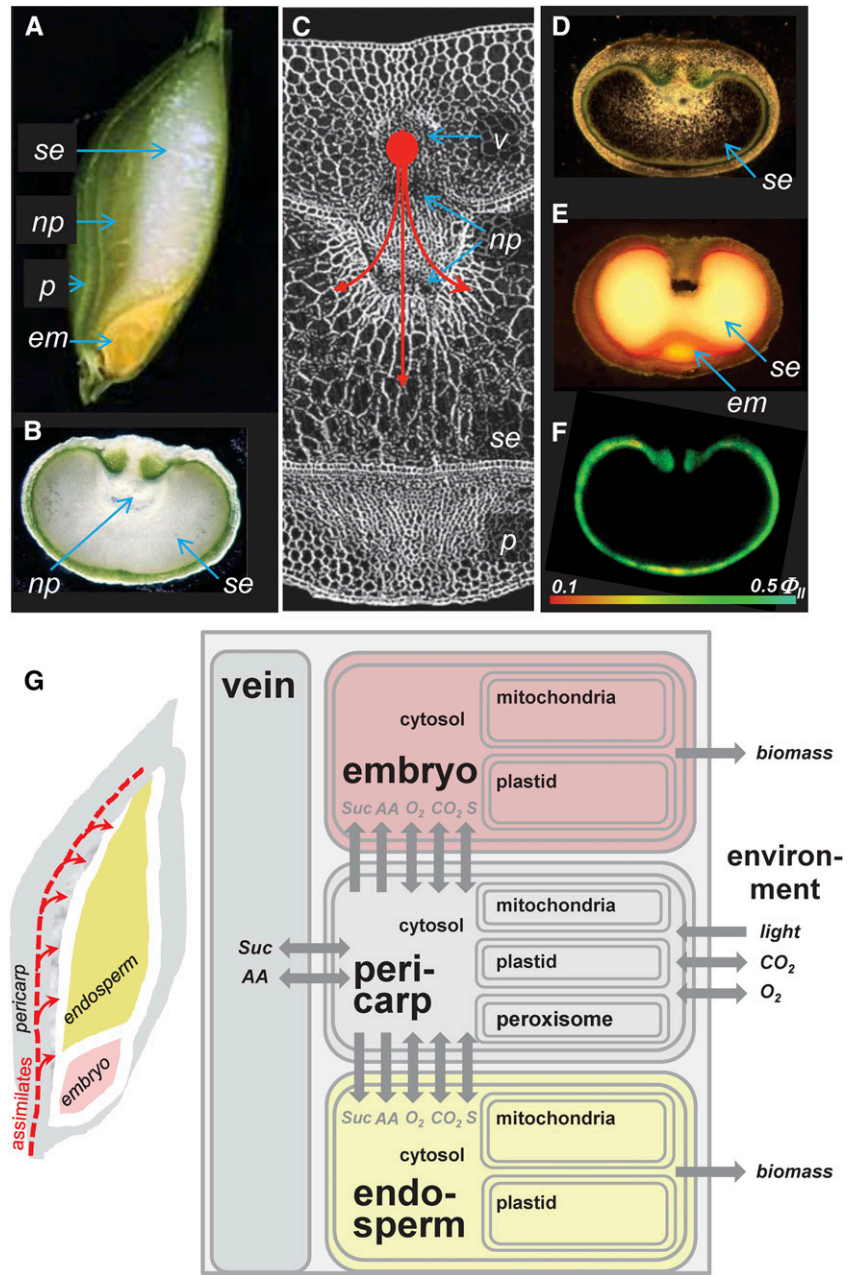
Model simulation and constraining (based on biomass equations, growth rate, and gas exchange rates used for parameter fitting) are detailed in "Materials and Methods." A fully detailed description of the multicomponent FBA model, comprising the full set of reactions, the experimental basis for each reaction, the modeling constraints, and the experimental data used for parameterization, are given in Supplemental Methods S1 and Supplemental Data Sets S1 and S2.

The Model Predicts Differential Flux Pattern and Light Responses within the Individual Grain Organs

The multicomponent FBA enabled us to predict the dynamic, metabolic architecture of grains; the log-ratio flux maps in Figure 4 illustrate the response of each organ to illumination. More detailed flux maps are given in Supplemental Figures S1 and S2, and the full set of flux values (including flux ranges) is listed in Supplemental Data Set S3.

In general, metabolic capabilities (defined by the underlying networks) and biomass composition, growth rates, etc.) differed markedly among grain components, which was reflected in the component-specific sub-models. The endosperm as the principal storage organ displayed the greatest substrate uptake, channeling the incoming Suc mostly into starch. The embryo receives less than 15% of assimilate passing through the pericarp and uses it to produce starch, proteins, and lipids. Finally, the pericarp is photosynthetically active and also experiences photorespiration and a daily starch turnover. A detailed description of the predicted component-specific flux patterns in response to illumination is given below.

Figure 3. Structural and metabolic heterogeneity of the developing barley grain and the corresponding FBA model. A, Longitudinal section. B, Transverse sections. C, The cellular structure of the crease region; red arrows indicate route of assimilate allocation. D, Starch distribution as shown by iodine staining. E, Lipid distribution (in red color) as shown by Sudan staining. F, Pulse amplitude modulation fluorescence image showing quantum efficiency in PSII (light-adapted state). G, The topological arrangement of the grain components and the corresponding FBA model. AA, Amino acids; em, embryo; np, nucellar projection; p, pericarp; S, sulfate; se, starchy endosperm; v, vein.



The Flux Pattern in Pericarp

The light response of the pericarp is dominated by unloading and redirection of Suc, photosynthetic CO₂ fixation, assimilate synthesis, photorespiration, and transient starch synthesis. The O₂ and assimilate are either recycled within the pericarp or exported to the endosperm and embryo. The tricarboxylic acid (TCA) cycle acts in noncyclic mode and provides carbon skeletons for nitrogen assimilation and reducing power. In the absence of light, photosynthesis/photorespiration is abolished and transient starch degradation sets in. The remobilization of starch results in the accumulation of Glc, which serves either as a precursor for Suc resynthesis or as a cyclic TCA substrate. Of the Suc fed into the filial tissues,

17.4% is derived from starch degradation (see below). However, this contribution is insufficient to compensate for the decreased supply of photosynthetically derived Suc (from the mother plant).

The Flux Pattern in Endosperm

The endosperm metabolism revolves largely around the storage of imported assimilate, primarily in the form of starch. The processing of Suc is catalyzed by Suc synthase and the cytosolic isoform of ADP-Glc pyrophosphorylase (AGPase; Fig. 4). Note that plastidial AGPase (pAGPase) in the endosperm is predicted to catalyze ADP-Glc. Glycolytic flux is largely restricted to the pyrophosphate-dependent phosphofructophosphatase

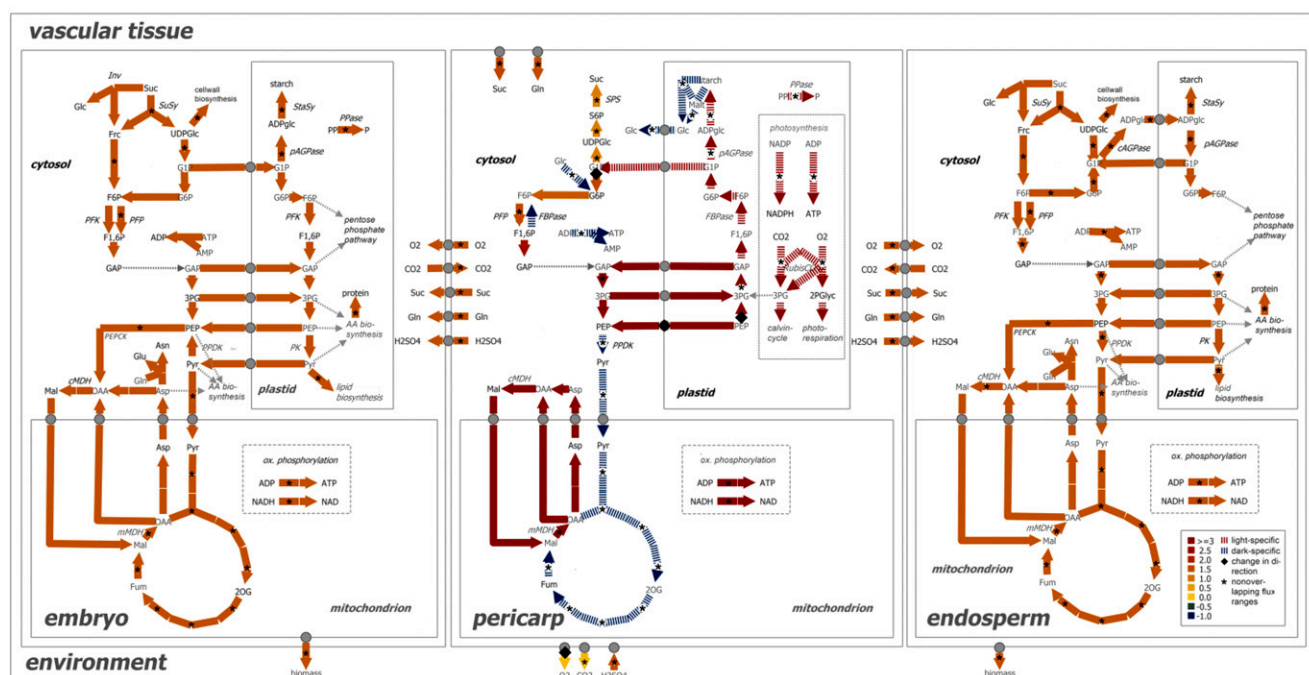
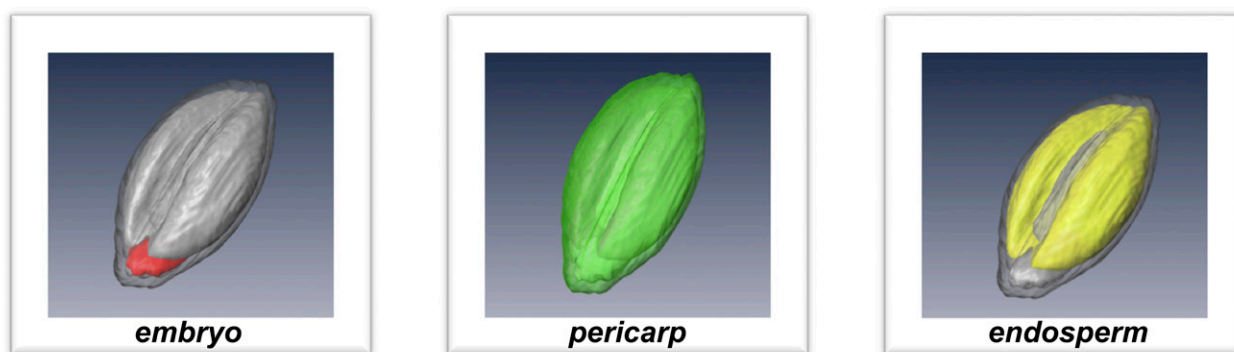


Figure 4. Predicted log-ratio flux maps (lit versus nonlit conditions) of the endosperm, embryo, and pericarp during the grain's main storage phase. Red dashed arrows indicate metabolic routes only active under lit conditions, and blue dashed ones indicate those exclusive to nonlit conditions. The direction of the metabolic flux indicated by arrowheads refers to flux under lit conditions. Changes in flux direction induced by the switch from lit to nonlit conditions are indicated by black diamonds. Numerical flux values (color coded) indicate x -fold changes in flux value, given as logratio of the simulated flux values of a given network reaction under lit versus nonlit conditions. Fluxes marked with an asterisk indicate fluxes with nonoverlapping flux ranges. The grain components (top sections) were derived from MRI-based models of grains imaged approximately 20 DAF. AA, Amino acid; *c*/mMDH, cytosolic/mitochondrial malate dehydrogenase; FBPase, fructose-1,6-bisphosphatase; Inv, invertase; PEPCk, phosphoenolpyruvate carboxykinase; PFK, ATP-dependent phosphofructokinase; PFP, pyrophosphate-dependent phosphofructokinase; PPK, pyrophosphate:pyruvate dikinase; PK, pyruvate kinase; StasY, starch synthase; SuSy, sucrose synthase.

and pyruvate phosphate dikinase. The TCA cycle acts in cyclic mode to provide energy, reducing equivalents and carbon skeletons for nitrogen assimilation. Under lit conditions, the increased Suc supply raises absolute flux values, including biomass accumulation (i.e. the metabolic fluxes differ greatly with respect to their flux value). However, the pathway utilization pattern remains stable (in clear contrast to the situation in the pericarp).

The Flux Pattern in Embryo

The embryo's pathway utilization pattern is unresponsive to the diurnal cycle (Fig. 4), thus fluctuations

in absolute fluxes are largely restricted to the effects of the light-induced variation in Suc supply. The pathway utilization pattern resembles that in the endosperm, with some notable differences (Fig. 5A): first, absolute flux values are much lower than in the endosperm, a feature related primarily to differences in Suc supply; second, in line with its biomass composition, the flux into starch and cell wall materials is less, while that into lipid/protein is greater; third, ADP-Glc synthesis is confined to the plastids (because the embryo lacks both cytosolic AGPase and an ADP-Glc transporter); fourth, the enzymes' plastidial pyrophosphatase (PPase), phosphoglucosmutase, and the glycolysis-related

phosphofruktokinase and aldolase are all active, whereas they are essentially inactive in the endosperm; and finally, respiratory activity is higher in the embryo.

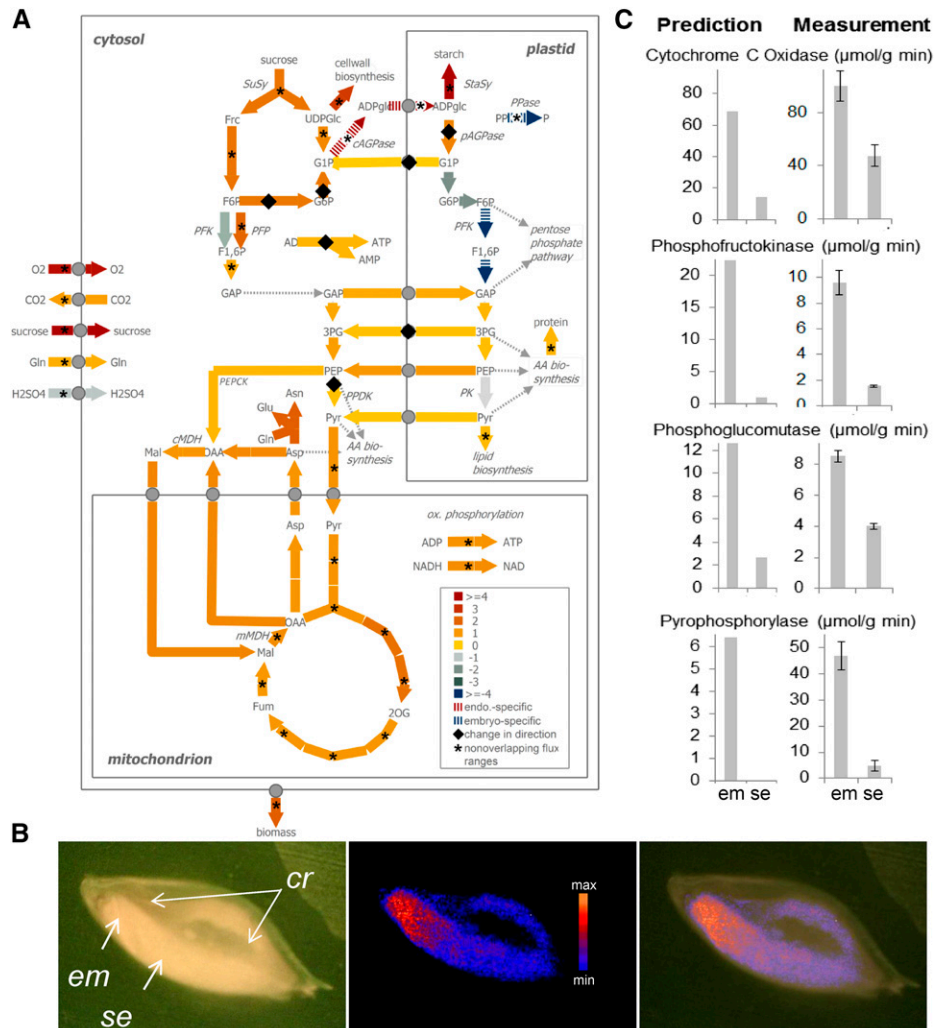
We tested some of the predictions in view of experimental data. Planar oxygen sensors designed to image oxygen consumption over time generated an output that was considered to mirror respiratory activity (Tschiersch et al., 2012). A respiration map of the barley grain generated in this way revealed that respiratory activity was much higher in the embryo than in the endosperm (Fig. 5B). Almost identical respiration maps were acquired for wheat grain (data not shown). When calculated O₂ consumption rates were compared to the model's predictions (taking cytochrome C oxidase as the major O₂-consuming flux), the experimental and simulated values proved to be well aligned (Fig. 5C). We further measured the maximum catalytic activity (V_{max}) of PPase, phosphofruktokinase, and phosphoglucomutase in crude extracts of dissected barley embryo and endosperm tissue. For all three enzymes, we found much higher activities in embryo versus endosperm tissues (Fig. 5C). Similar ratios in enzyme activity have been derived from model

predictions (following conversion of absolute flux values [$\mu\text{mol h}^{-1}$; Supplemental Data Set S3] in relative values [$\mu\text{mol g}^{-1} \text{min}^{-1}$]). Please note that the measured values provide maximum catalytic activities, which does not necessarily reflect the actual (in vivo) flux predicted by the model.

Pericarp Photosynthesis Supports High Grain Carbon Conversion Efficiency

The predicted carbon conversion efficiencies (CCEs) of the three grain components varied (Table I). The enclosure of the nonphotosynthetic endosperm and embryo by the pericarp supports the refixation of approximately 79% of the endogenously released CO₂, ultimately allowing the grain's CCE to reach approximately 95% under lit conditions. Rubisco contributes most significantly to this high CCE (Supplemental Data Set S3). Pericarp photosynthesis relies exclusively on the respiration of the filial tissues for its CO₂ supply. Photosynthetic O₂ production generates a net export of O₂ under lit conditions and provides sufficient O₂ to

Figure 5. Contrasting metabolic processes in the barley endosperm and embryo. **A**, A log-ratio flux map depicts central metabolic processes operating under lit conditions. Red and blue dashed arrows indicate metabolic routes exclusively active in, respectively, the endosperm and the embryo. Flux direction as indicated by arrowheads refers to endosperm-specific flux. Changes in flux direction are indicated by black diamonds. Numerical flux values (color coded) indicate x-fold changes in flux value, given as logratio of the simulated flux values of a given network reaction in the endosperm versus embryo. Fluxes marked with an asterisk indicate fluxes with nonoverlapping flux ranges. **B**, Respiration mapping across the grain using a planar oxygen sensor. The left section shows a grain cross section, and the right section shows the derived respiration map based on the fluorescence signal emitted by the sensor (red indicates peak respiratory activity). **C**, Enzyme activities predicted from the FBA model (under lit conditions) compared with experimentally determined V_{max} values in extracts of the embryo (em) and starchy endosperm (se) and as derived from the respiration map shown in B. cr, Crease.



meet the metabolic demand of both the endosperm and embryo. CO₂ fixation in both the embryo and endosperm is mediated largely by phosphoenolpyruvate carboxykinase, although at a much lower rate than occurs in the pericarp (Supplemental Data Set S3). The CCEs of the nongreen embryo (67.1%) and endosperm (85.3%) were not responsive to illumination, and the differences between these two organs reflected the differences in their biomass composition (the higher lipid content of the embryo induces a lower CCE). Suc allocation within the grain was strongly affected by light: it was 0.05 $\mu\text{mol h}^{-1}$ in the dark and 0.23 $\mu\text{mol h}^{-1}$ in the light (Table II). While most of these light-dependent differences can be related to changes in Suc flux from the maternal plant to the pericarp, some 9.4% of the Suc in the pericarp was endogenously synthesized.

Light-Enhanced Solute Flux toward the Ear Is Coupled with Metabolic and Molecular Adjustments in the Grain

While the molecular and metabolic responses of barley grains to diurnal cycles have been analyzed in detail (Mangelsen et al., 2010), here, we focused on shorter time scales (6 h) using the shielding approach (as demonstrated in Fig. 1, A and B) combined with isotope feeding. Cut stems were provided with ¹⁴C-labeled Suc, and the ¹⁴C content of and its partitioning within the grain were monitored. The provision of light prompted a significant increase (25% \pm 9%) in the uptake of ¹⁴C Suc (Fig. 6A). About 20.0% of the label was associated with starch, about 7.5% with protein, about 1.5% with the cell wall, and about 0.9% with the lipid fraction (the remaining label was found in the soluble fraction). The only fraction that was statistically significantly altered by the light conditions was the cell wall component, which was reduced in the absence of light. In a similar experiment based on ¹⁵N-labeled Gln, the stimulation in uptake generated by light was 39% \pm 9% (Fig. 6A).

At the level of metabolites, the liquid chromatography/mass spectrometry analysis suggested that despite the light-stimulated uptake of Suc, its steady-state level in the grain remained unchanged, irrespective of the lighting regime (Fig. 6B). Meanwhile, the provision of light reduced the abundance of both the glycolysis

Table I. Model-predicted effect of light availability on CCE in barley seed organs

Organ	C Uptake ^b		CO ₂ Efflux		CCE	
	Dark	Light	Dark	Light	Dark	Light
	$\mu\text{mol h}^{-1}$				%	
Embryo	0.115	0.481	0.038	0.158	67.1	67.1
Endosperm	0.583	2.428	0.086	0.358	85.3	85.3
Pericarp	0.708	3.169	0.137	0.132	80.6	95.8
Seed ^a	0.584	2.653	0.137	0.132	76.5	95

^aMulticomponent seed model composed of embryo, endosperm, and pericarp. ^bUptake of Asn, Gln, Suc, and CO₂ (CO₂ is only taken up by the pericarp).

Table II. Model-predicted effect of light availability on Suc allocation within the grain

Suc allocation is defined as the sum of pericarp-specific Suc import (Suc allocation from the vascular tissue to the pericarp) and pericarp-specific Suc synthesis (catalyzed via the enzyme Suc-P-synthase).

Reaction	Dark		Light	
	$\mu\text{mol h}^{-1}$	%	$\mu\text{mol h}^{-1}$	%
Suc import	0.05	82.57	0.21	90.64
Suc synthesis	0.01	17.43	0.02	9.36
Sum	0.05	100.00	0.23	100.00

entry substrates (Glc- and Fru-6-P) and end products (pyruvate) and the intermediates of the TCA cycle. There was also a reduction in the levels of AMP, lactate (fermentation product), most free amino acids, ADP-Glc (starch precursor), and trehalose-6-P (sugar-signaling molecule). Only three of the 36 metabolites assayed were markedly affected (>50% change in concentration) by the provision of light.

To check for possible changes to the pattern of Suc distribution across the grain, we applied an MRI-based imaging approach to ear-shielded grains. It revealed that, irrespective of the lighting regime, the Suc concentration was high throughout the crease region, including the endosperm cavity (Fig. 6C). The largest concentrations were noted within the vascular tissue. Thus, the distribution pattern of Suc was not influenced by the light conditions.

A transcriptomic analysis of the grains (using 12K complementary DNA [cDNA] arrays) from the ear-shielding experiment revealed that exposure to light up-regulated 53 genes and down-regulated 44 genes (Supplemental Data Set S4). In parallel, a set of 16 genes (Table III) was subjected to quantitative reverse transcription (qRT)-PCR analysis; the combined data revealed that the transcript abundance of only a rather small number of genes involved in primary metabolism was changed. Genes up-regulated by light included one encoding the plasma membrane-localized Suc transporter SUT1, one encoding starch-branching enzyme1, one encoding a plastidial triosephosphate/phosphate translocator, one encoding the pericarp-specific Rubisco small subunit, and a few sugar/energy metabolism-related genes (trehalose-6-P phosphatase); the down-regulated ones comprised genes involved in Suc cleavage (cell wall-bound invertase), energy metabolism (alcohol dehydrogenase, aldolase, and glyceraldehyde 3-P dehydrogenase), and lipid storage (oleosin).

DISCUSSION

Maximizing carbon and energy use efficiency is key to crop improvement, but these rather straightforward physiological concepts are underlain by a complexity of molecular and metabolic processes, including their compartmentation within the living plant. This study aims to characterize the spatial heterogeneity of the grain's metabolism and especially to assess the

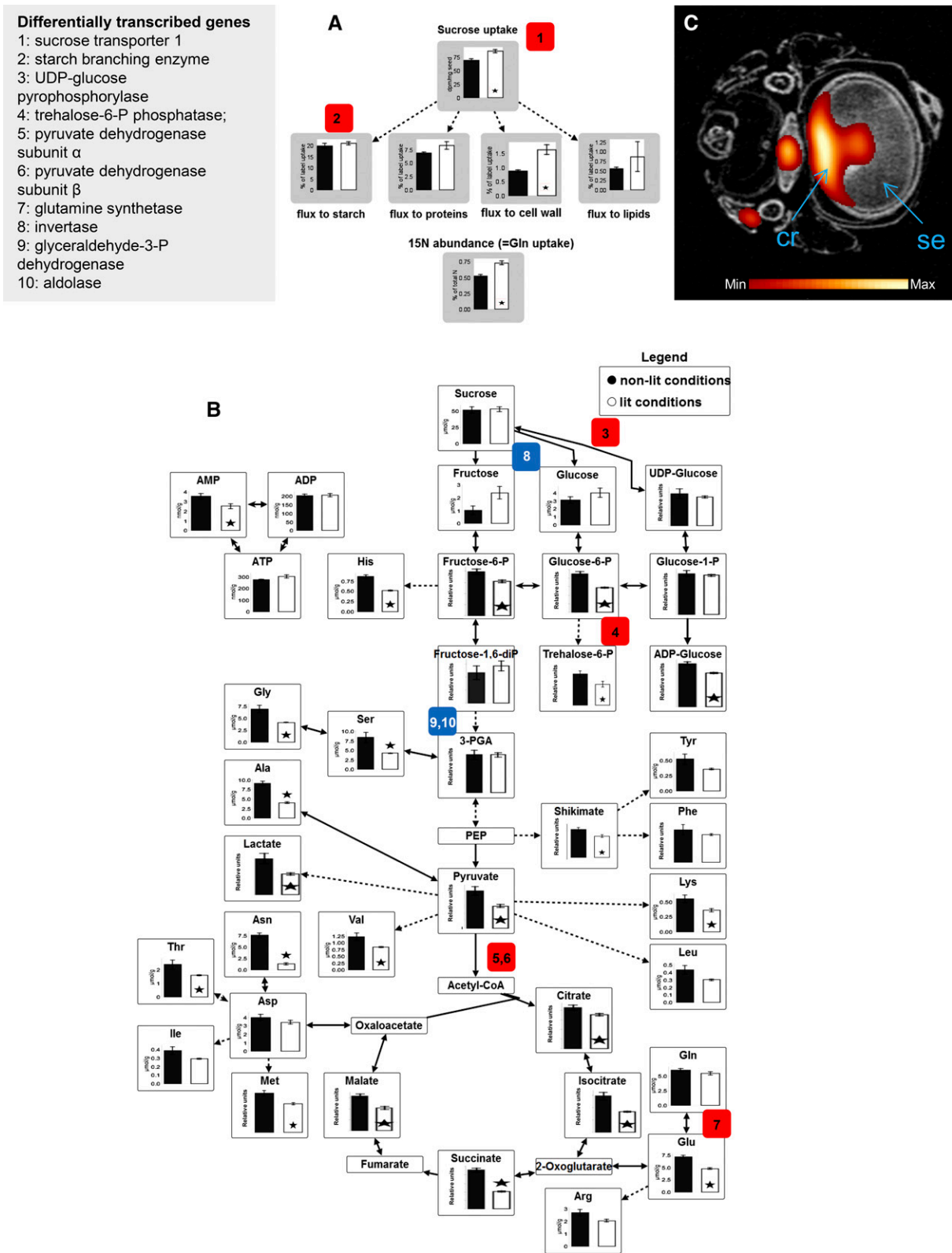


Figure 6. The light responses of the barley grain during ear shielding. A, The uptake of ^{15}N Gln and ^{14}C Suc into the intact grain, and the partitioning of ^{14}C -label into the three grain components. B, Steady-state metabolite levels as measured by liquid chromatography/mass spectrometry. Data given in the form mean \pm SE ($n = 6$). Asterisks indicate statistically significant ($P < 0.05$) differences according to a Student's t -test. Changes in transcript abundance are indicated in red (up-regulated under lit conditions)

Table III. List of genes analyzed by qRT-PCRs for their expression under light conditions compared with the dark during mid to late grain-filling phase (18 d after flowering)

Clone ID ^a	Gene Identification	Fold Change in Expression under Light ^b	Preferential Tissue Localization of Gene Expression ^c
Genes, up-regulated under light conditions			
AJ272309	SUT1, plasma membrane localized	1.74***	Endosperm
FN179382	Starch branching enzyme (SBE1)	1.46***	Endosperm
BQ472366	Small subunit of ribulose-bisphosphate carboxylase	1.45***	Pericarp
JX878491	Gln synthetase (GS1), cytosolic	1.29***	Pericarp
CA022884	Pyruvate dehydrogenase E1, α -subunit	1.72**	Ubiquitous
X91347	UDP-Glc pyrophosphorylase	1.50*	Endosperm
BQ469324	Pyruvate dehydrogenase E1, β -subunit	1.27*	Ubiquitous
Genes without changes in expression levels between light and dark conditions			
X69931	Suc synthase2	1.66	Endosperm
AJ272308	SUT2, vacuolar	1.20	Endosperm
AY483150	Cellulose synthase A1	1.20	Ubiquitous
AY483152	Cellulose synthase A2	1.20	Pericarp, late endosperm
AL507830	Glycerol-3-P dehydrogenase, NAD+	1.01	Embryo
Z26322	Ala aminotransferase	0.88	Endosperm
Genes, down-regulated under light conditions			
BQ468368F	Cell wall invertase	-2.68*** to -1.48	Endosperm
J403592	Fru 1,6-bisphosphate aldolase	*	Embryo

^aEMBL/GenBank accession numbers. ^bThe data correspond to the analysis of three biological \times \geq three technical repetitions; *, Student's *t* test significance at $P < 0.05$; **, Student's *t* test significance at $P < 0.01$; and ***, Student's *t* test significance at $P < 0.001$. ^cThe data about tissue-specific localization of the respective gene expression were extracted from Sreenivasulu et al. (2006).

metabolic capacity and efficiency of individual grain organs in the face of a fluctuating environment. Our data suggest that the grain employs a set of distinct metabolic strategies to deal with both diurnal and environmental variation in incident light and the consequential variation in the supply of assimilate to the ear.

The Ear and Caryopsis Respond to Illumination by Adjusting Their Solute Flux

As the grain is a sink organ throughout its development, a consistent supply of assimilate is a high priority. The source of this assimilate (Sanchez-Bragado et al., 2014), its routing (Melkus et al., 2011), and the variability in its supply rate (Matsushashi et al., 2006) have all been investigated in some detail but are still under debate. To explore the dynamics of solute flow toward cereal grains, this study harnessed unique NMR-based technology (Kartäusch et al., 2014). Our NMR method enabled us to monitor flux in the peduncle of wheat and barley during many days in vivo. Results demonstrate net solute flow directed toward the ear/grain and flow velocities altering according to the photoperiodic (diurnal) cycle (Fig. 1). Analysis of assimilate transport in wheat using a ¹¹C positron-emitting tracer likewise indicated an important role that the photocondition of the ear plays in the transportation of photoassimilates (Matsushashi et al., 2006). We conclude

that the diurnal cycle has a profound effect on the metabolic behavior of the cereal grain.

An unexpected rapid response to shielding the ear was the abolition of solute flow (Fig. 1), the implication of which is that the ear/grain cannot be merely a passive receiver of assimilate but rather must have developed its own means of regulating solute flow. The relevant underlying mechanism(s) remain obscure, but their effect is to provide the individual ear/grain a measure of autonomy in controlling its import of assimilate and thereby its metabolism.

The light-dependent velocity of solute flow within the peduncle was accompanied by changes to the MRI parameter T2 in the grain (Fig. 2A). Relaxation time (T1 and T2) is a highly reliable surrogate for water distribution/state in both plant (Van As and van Duynhoven, 2013) and animal (Hueper et al., 2013; Wu et al., 2014) tissue. In living plant tissue containing vacuolated cells, the majority of the water present is contained in the vacuoles, and as a result, T2 images are dominated by vacuolar water (Van As et al., 2009). Thus, increases over time in T2 probably reflect increases in vacuolar size (Metzner et al., 2014). Here, light-induced changes in T2 were shown to occur within the crease region (Fig. 2B), which is the primary entry point into the grain for not only solutes (Melkus et al., 2011), but also water (Jenner et al., 1988). Given this, it becomes reasonable to suggest that the response

Figure 6. (Continued.)

and blue (up-regulated under nonlit conditions). 3-PGA, 3-Phosphoglyceric acid; diP, diphosphate; PEP, phosphoenolpyruvate. C, Steady-state distribution of Suc under lit conditions, as measured by MRI. cr, Crease; se, starch endosperm.

to light includes an increased flow of water into the grain. The simultaneous influx of both water and solutes toward/within the grain is biologically meaningful because assimilate is transported in aqueous form, and thus changes in solute flow imply changes in water flow. The proposition is therefore that water and assimilate uptake into the grain are tightly coupled with one another via a mechanism(s) as yet unknown. Future studies may help to clarify whether the source of this water is from the xylem or from the phloem and/or whether light-controlled aquaporins (Prado et al., 2013) are involved in regulating the process.

Orchestration of Organ-Specific Metabolic Responses

Suc and light are the orchestrators of the metabolic activity of the grain. Assimilate flux in the pericarp was highly sensitive to incident light, while both the endosperm and the embryo responded more proportionately, at the same time leaving pathway utilization patterns largely unaltered (Fig. 4). What is the primary signal for these metabolic responses? Light signals seem to have an infinite spectrum of possibilities (Chory, 2010), including numerous links to phytohormones and sugars (Lau and Deng, 2010; Sairanen et al., 2012). A plausible hypothesis is represented by the idea that enzyme capacity in central metabolism is in large excess and that flux regulation propagates rapidly via simple mass action across the network, controlled by the ratio between the various enzymes' product and substrate concentrations. Allosteric and redox control of enzyme proteins is another possibility to link light/Suc availability with metabolic activities (Michalska et al., 2009; Schwender et al., 2015). These hypotheses chime with the recent finding that flux regulation in central metabolism of seeds is unlikely to reflect transcriptional activity (Schwender et al., 2014). In principle, trehalose-6-P could act as the instantaneous signal of sugar availability, but the response observed in the shading experiment (a light-induced decrease in trehalose-6-P level and a corresponding stimulation of trehalose-6-P phosphatase transcript) is the opposite of what is generally expected when the availability of sugar rises (Smeekens et al., 2010).

The metabolic and molecular response of grains in ears from which light had been excluded (Fig. 6; Table III) differed significantly from those observed in the course of a normal night (Mangelsen et al., 2010). While during nighttime numerous changes in transcript abundance occur, only a limited number of transcripts (including, notably, the major Suc transporter SUT1) were affected by ear shielding, and there was little perturbation either in the steady-state levels of major metabolites or to the pattern of sugar distribution within the grain. Clearly, the decline in the supply of Suc imposed by a 6-h period of ear shielding can be readily compensated for, establishing a strong homeostasis with respect to both the level and distribution of sugar. The aspect of homeostasis could be very relevant

because fluctuating sugar levels could lead to unwanted effects on Suc-mediated control circuits (Rahmani et al., 2009), causing energy-costly transcriptional/translational reprogramming. The proposition is that short-term changes in the supply of Suc imposed by environmental fluctuation are evened out via (posttranslational) metabolic control. Network stability mechanisms have been demonstrated in a number of diverse plant systems: some examples are provided by the response to alterations in the supply of Glc (Rontein et al., 2002), oxygen (Williams et al., 2008), and light (Borisjuk et al., 2013). These may represent the key to ensuring a robust and energy-efficient physiological homeostasis.

The Grain Grows Preferentially during the Lit Period

When growth is considered to be an increase in biomass over time, the indication is that the developing grain grows preferentially in the light, coinciding with the period when its sugar uptake is at its maximum. The intake of sugar in turn induces a high level of metabolic activity, much of which is directed to converting sugar into biomass (preferentially starch). The light response also included a presumably higher water uptake and a higher partitioning of sugar into the cell wall (Fig. 6A), which may reflect the light-induced transcriptional activation of both cell wall synthesis and expansion (Mangelsen et al., 2010). Thus, grain growth appear to be favored during the daytime, in agreement with the finding that fruits grow more rapidly during the day than during the night (Guichard et al., 2005).

The Grain as a Synergistic Metabolic and Architectural System

During early phase of grain development, the pericarp functions as an assimilate sink (Radchuk et al., 2009). It largely degenerates toward maturation while the chlorenchyma layer and crease region remain alive till desiccation (Tran et al., 2014). At the mid stage (as sampled here), it somehow behaves as if it were an autotrophic leaf enveloping the heterotrophic storage organs. Three characteristic processes are involved. First, the starch, accumulated largely in chlorenchyma tissue of pericarp during the lit period, is degraded during the night. This pattern echoes the diurnal regulation of β -amylases (Mangelsen et al., 2010) and is characteristic of source leaves. Second, peak PSII electron transport rates are equivalent to those prevailing in the flag leaf (Tschiersch et al., 2011), a level that is much higher than has been recorded in the green seeds of a number of dicotyledonous species (Borisjuk et al., 2005, 2013). And finally, as in the leaf, the lit period features noncyclic rather than cyclic TCA activity. Noncyclic TCA fluxes have been noted as being characteristic of the illuminated leaf (Sweetlove et al., 2010; Cheung et al., 2014), while in contrast, cyclic flux is important in heterotrophic tissues such as the endosperm and embryo. The pericarp differs anatomically from the leaf in

its substantially lower frequency of stomata in the epidermal layer (Cochrane and Duffus, 1979). This feature ties in well with the model's prediction that photosynthesis in the pericarp relies exclusively on endogenously released CO₂, having no requirement for the uptake of any atmospheric CO₂ through the stomata.

The FBA model predicted that pericarp photosynthesis is of high relevance in terms of carbon refixation. The estimated CCE of the barley grain (approximately 95%) exceeds that of maize (*Zea mays*) endosperm (76%–92%; Alonso et al., 2011). Although there is little compositional difference between the barley and the maize grain, the latter does not benefit from photosynthesis-related CO₂ refixation. The estimated CCE of other nongreen seeds (Alonso et al., 2007) and green seeds (Goffman et al., 2005; Allen et al., 2009; Borisjuk et al., 2013) is lower still. The conclusion is that the architecture of the developing barley grain, and by inference, also that of wheat, rice (*Oryza sativa*), and oat (*Avena sativa*), is one important key to its high CCE and thus to the crop's yield potential.

Implications for Crop Improvement

The small-grain cereal caryopsis appears to be an almost perfect entity for carbon storage; with a CCE of approximately 95%, there seems to be little room for any improvement in efficiency. Thus, the emphasis needs to be put on stimulating the supply of assimilates to the developing grain rather than on attempting to manipulate grain metabolism.

The pericarp's photosynthetic activity makes a contribution to the energy/carbon balance of the grain. It might therefore be advantageous to stimulate its capacity, which is already high but spatially confined to a narrow band within the pericarp.

Illumination not only stimulates photosynthetic activity, but also prompts solute/water fluxes in general. Thus, fast acclimation to changing light supply could be key to high energy and carbon efficiency. The developing grain benefits from the capacity to anticipate a burst of sugar arriving via the phloem, because this facilitates the grain's rapid adjustment to its synthesis of storage products. Improvement of the adaptive abilities should be considered in the context of both structural and functional organization of the grain, ear, and/or whole plant.

Flux maps have provided several striking predictions, e.g. pAGPase in the endosperm catalyzes the degradation of ADP-Glc. The unexpected conclusion would be that the endosperm-specific down-regulation of pAGPase may have the effect of increasing the grain's starch content. This contradicts the commonly held view that carbon entering the plastid in the form of ADP-Glc is committed to starch synthesis and cannot be diverted into other metabolic pathways (James et al., 2003). The present prediction is supported by the demonstration that pAGPase in the barley endosperm catalyzes a readily reversible reaction in vivo (Tiessen et al., 2012). A likely scenario is therefore that endosperm

pAGPase represents a metabolic valve, which, depending on metabolite concentrations, can divert carbon away from starch synthesis. While experimental validation is needed, we conclude that the application of modeling tools can provide useful predictions for further experimental work.

Potential Limitations of Our Modeling Approach

The predictive power of FBA models highly depends on the accuracy of data used for reconstruction and parameterization (i.e. constraints). With respect to model reconstruction, the main factors potentially affecting the precision of flux estimation comprise the simplification of not taking into account (1) organ-specific genome-scale models and (2) different cell types in the modeled grain components. With respect to model parameterization, uncertainties are due to the lack of experimental data and result in the need for parameter estimation. In this study, maintenance energy/reductant costs were estimated by fitting the model to experimentally measured gas exchange rates. Maintenance costs were assumed to be the same under lit/nonlit conditions and in the different grain tissues. As energy demand can have substantial effect on predicted flux distribution (Poolman et al., 2009; Cheung et al., 2013), these simplifications can be assumed to have the strongest effect on prediction quality compared with the remaining constraints applied in this study. However, neglecting maintenance cost (as done by many plant metabolic models) would have resulted in an even greater potential uncertainty. Parameter assumptions having a lesser effect on the accuracy of model predictions are related to (1) biomass composition (lit = nonlit), (2) starch degradation/biosynthesis in the pericarp (rate of biosynthesis = rate of degradation), and (3) Rubisco: ratio of oxygenase to carboxylase (taken from literature).

The accuracy of FBA models also depends on the choice of the objective function, although to a lesser extent than the constraints (Cheung et al., 2013). In line with other studies, in this study, the efficient use of carbon sources was assumed to be the main objective of metabolism. The objective was computed as a two-step optimization process (first, minimize Suc/Asn/Gln uptake, and second, minimize the overall intracellular flux). The biological assumption underlying this is that the barley caryopsis grows while (1) using the minimal amount of carbon, resulting in carbon efficiency, and (2) achieving an efficient channeling of metabolites. Good agreement has been reported between the predicted and measured fluxes for heterotrophic plant metabolism using the first (Hay and Schwender, 2011) and second objective function (Cheung et al., 2013), respectively. Compared with other objective functions applied in nonplant FBA studies (maximization of biomass or minimization of energy requirements), the chosen objective function seems to best represent the overall objective of the mixotrophic nature of the barley caryopsis.

Despite the uncertainties in modeling constraints discussed above, the predicted flux distributions reflect the success of the objective function and modeling constraints in capturing a realistic picture of the metabolic architecture of cereal grains. We believe that exploring the metabolic architecture of cereal grains could open new avenues for crop improvement.

MATERIALS AND METHODS

Plant Growth

Barley (*Hordeum vulgare*) 'Barke' and wheat (*Triticum aestivum*) 'Certo' plants were cultivated in growth chambers under a 16-h-light/8-h-dark regime at 20°C/14°C. Supplemental light was set to an intensity of approximately 600 $\mu\text{mol quanta m}^{-2}\text{s}^{-1}$ (at approximately 1 m above ears). Flowering ears were tagged for determination of DAF.

NMR Tools and Methods

Flux Measurements Using Low-Field NMR Instruments

Long-term measurements of flux toward the spike were performed using a home-built mobile MRI scanner with 0.5 Tesla (T) and a conventional driveL console (Pure Devices GmbH). The light level used during NMR experiments corresponds to that in the greenhouse. Velocity profiles were acquired using the AC-gradient method described by Walton and Conradi (1987). A solenoid coil with a height of 2 mm was used for transmit/receive. The diameter of the solenoid coil was fitted to the size of the stem. The number of echoes was set to 372, and 1-ms gradients with a magnitude of 0.2 T m^{-1} were applied. The measurement was performed as a single shot measurement. However, due to the very low signal-to-noise ratio, the measurement was averaged 10 times, and the calculated mean flux change was averaged over 10 complete measurements. Therefore, the total measurement duration for a single point of the flow trend lasts approximately 3 min. In conclusion, the monitored net flow is the difference between solute flow and the negligible perpendicular flow within the measured volume. The measured signal is created in large part by water protons but also by the protons attached to the sugar molecules and further constituents. All details are explained in Kartäusch et al. (2014).

Imaging Experiments Using High-Field NMR Instruments

Imaging experiments on the entire spike were performed on a Bruker Avance 17.6 T wide-bore (89-mm i.d.) superconducting magnet (747.6 MHz; Bruker BioSpin) equipped with a 1,000 mT m^{-1} gradient system and a custom-built birdcage coil with 20-mm i.d. A glass fiber connected to the custom-built light source and operated automatically by timer clock was used for setting a fixed light-dark interval during experiments in the 17.6 T NMR instrument. The image acquisition was performed by the following settings: the longtime monitoring of the spike during dark-light switches was performed based on the repeatable three-dimensional imaging using a multislice multiecho sequence for acquisition of three-dimensional data sets. Repetition time was 800 ms, echo time was 5.886 ms, and number of echoes per data set was 12. For each echo, a $192 \times 96 \times 96$ matrix was acquired. The total scan time of a three-dimensional data set was 2 h and 3 min. The Suc imaging experiments were performed using the slice-selective geHMQC sequence (for details, see Melkus et al., 2011).

Data Processing

The acquired raw data sets were processed in MATLAB R2013a (MathWorks). Using an in-house written computer program, the k-space data were Fast Fourier transformed to image space, and T2 maps were calculated by fitting the multiecho images pixel wise (i.e. for each pixel of the image, the data were processed individually) to a monoexponential function. The T2 values shown in Figure 2A are averaged over three time steps belonging to one darkness/light period. For statistical analysis in Figure 2A, the number of voxels used for calculation of the T2 values was 141 (white), 160 (yellow), and 174 (blue and green). A mask (Fig. 2B) was used on the resulting three-dimensional data sets containing the calculated T2 parameters. Commercial software Amira 4.1

(Mercury) was used for the overview of seed internal structure as well as for segmentation and preparation of figures.

Data Acquisition for FBA Model Parameterization and Fitting

Intact grains were taken at distinct developmental stages for manual dissection of endosperm and embryo, followed by weighing (fresh and dry weight) to determine growth rates. We also analyzed soluble sugars/free amino acids (Rolletschek et al., 2005), fatty acid composition (Borisjuk et al., 2005), and total content of starch, lipid, and protein (Borisjuk et al., 2013). Gas exchange measurements were done by incubating freshly harvested, intact grains in buffered solution (50 mM Gln, 50 mM Suc, and 10 mM MES buffer, pH 6.2) in closed flasks for up to 2 h at 20°C. During this time, the oxygen and carbon dioxide concentration inside the flasks was continuously monitored using sensor spots (O_2 : PSt3 and CO_2 : SP-CD1-D5-rMy-US; PreSens GmbH) inside the flasks connected via fiber optic cables to transmitters (Fibox-3; pCO2 mini; PreSens GmbH). Incubation started with nonlit conditions, followed by step-wise increases in light supply using the lightning system of a microscope (each time period, 5–10 min; Schott). Rates for O_2/CO_2 uptake (release) were determined from the change in sensor signal over time using linear regression models. Data on the photosynthetic electron transport (PSII) in the pericarp were taken from pulse amplitude modulation fluorescence analysis published earlier (Tschiersch et al., 2011).

Flux Balance Analysis

To predict component-specific metabolic fluxes under lit and nonlit conditions, the multicomponent model was analyzed using FBA with the objective function and constraints specified below.

Objective Function

Assuming that developing barley grains make the most efficient use of their carbon sources, the minimization of Suc/Asn/Gln uptake per flux unit was used as the objective function for all FBA simulations. The objective was computed as a two-step optimization process, where the first step is to minimize the pericarp's uptake of Suc, Asn, and Gln and the second step is to minimize the overall intracellular flux.

Constraints

Model simulation under lit conditions was performed by fixing the endosperm- and embryo-specific growth rate according to experimentally determined rates (endosperm, 0.06 mg h^{-1} ; and embryo, 0.007 mg h^{-1}). Tissue-specific maintenance energy/reductant costs (endosperm, 0.3152/0.0004; embryo, 0.0925/0.0002; and pericarp, 6.4415/0.0266 [ATP/NADPH drain in $\mu\text{mol h}^{-1}$]) were estimated and constrained by fitting the model to experimentally determined gas exchange rates under lit conditions. In the pericarp, the uptake of light was constrained to 16 $\mu\text{mol h}^{-1}$ according to experimentally determined rates of photosynthetic electron transport. The flux ratio of Rubisco (oxygenase-to-carboxylase reaction) was set to a ratio of 30:70 according to barley-specific data reported in the literature (Skillman, 2008). In addition, the ratio of starch biosynthesis to Suc biosynthesis was set to a ratio of 50:50.

Model simulation under nonlit conditions was performed by fixing the tissue-specific growth rates (endosperm, 0.014 mg h^{-1} ; and embryo, 0.0017 mg h^{-1}) according to estimates resulting from fitting the model to gas exchange rates under nonlit conditions. Assuming that maintenance costs do not vary between lit/nonlit conditions, tissue-specific maintenance energy/reductant costs were fixed according to 60% of total ATP consumption and 1% of NADPH consumption (endosperm, 0.0757/0.00009; embryo, 0.0222/0.00005; and pericarp, 0.0187/0.0 [ATP/NADPH drain in $\mu\text{mol h}^{-1}$]). Due to the lack of experimental data, the rate of starch degradation was fixed to 0.0213 according to the rate of starch synthesis predicted by the model under lit conditions.

Flux Ranges

Flux ranges were calculated using flux variability analysis (Mahadevan and Schilling, 2003). The predicted fluxes were considered to significantly differ between conditions if their flux ranges did not overlap (for details, see Supplemental Methods S1).

A fully detailed explanation of the process of model reconstruction, parameterization, and analyses are given in Supplemental Methods S1 and Supplemental Data Sets S1 and S2.

Oxygen Imaging

For analyzing the local respiration rate in embryo versus endosperm, we used a fluorescence ratiometric-based device, consisting of an oxygen-sensitive foil and a USB microscope (for details, see Tschiersch et al., 2012). Briefly, the grain was cut in two halves, and the sensor foil was placed on the sample surface. The sample/sensor foil was kept in darkness. Based on the localized change in fluorescence signal (which equals oxygen concentration) over time (5 min), the local oxygen consumption can be estimated.

Enzyme Activity Assays

All enzyme assays were done in grain extracts using the UVIKON XL spectrophotometer (GOEBEL Instrumentelle Analytik GMBH). Activity of the enzyme PPase was determined according to Jonik et al. (2012). Assay conditions for the determination of phosphofructokinase and phosphoglucomutase were taken from Gibon et al. (2004). All assays were checked to be dependent on each substrate and linear with respect to time and amount of extract.

Experimental Design to Study the Light Response of Grains

Intact ears were kept in either light (600 μ E) or darkness (enclosed with black paper), while the remaining part of the plant was fully illuminated (600 μ E). The experiment started during light phase at 8 AM. After a 6-h period, grains (approximately 18 DAF) were quickly removed, immediately frozen in liquid N₂, and stored at -80°C until used for further metabolite and transcript analysis.

Metabolite Analysis

Metabolic intermediates were extracted and analyzed exactly as in Rolletschek et al. (2005).

Transcript Analysis

Total RNA was extracted from treated and control grains using the Trizol reagent (Invitrogen), as described earlier (Radchuk et al., 2011), and treated with DNase. For cDNA array analysis, RNA was reverse transcribed and used for the synthesis of ³³P-dCTP-labeled probes. Probe preparation, hybridization, and processing of 12K barley seed cDNA arrays were done essentially as described (Sreenivasulu et al., 2006). Images of hybridized nylon membranes were subjected to automatic spot detection using the MATLAB program. Signal intensities of 11,787 genes were scored from the double spots, enabling us to assess two replications. Additionally, two biological repetitions were performed using RNA from independently grown and treated grains. Quantile normalization (Bolstad et al., 2003) was carried out on the complete data set. Fold changes between wild-type and treated probes were calculated from the replicates. *P* values were calculated based on a moderated Student's *t* test to detect false positives. Genes that showed statistically significant differences in expression under light conditions compared with wild-type grains at the level 1.5-fold and higher in both biological replications were selected for further analyses. For qRT-PCR, 5 μ g of the total RNA was reverse transcribed by SuperScript III reverse transcriptase (Invitrogen) with the oligo(dT) primer. The resulting cDNAs were used as a template for qRT-PCR analyses, which were performed as described (Radchuk et al., 2011). Primer sets for each gene have been selected as recommended by Udvardi et al. (2008) and are listed in Supplemental Data Set S5. Experiments were run using three biological replications with at least three technical repetitions per replication. Dissociation curves confirmed the presence of a single amplicon in each PCR. The cycle threshold (Ct) of each gene of interest from each sample was normalized against endogenous reference gene *actin* and calculated as an arithmetic mean of the replicates. The relative gene expression levels in treated versus control grains and the fold changes of gene expression values were presented as 2^{- $\Delta\Delta$ Ct} according to Livak and Schmittgen (2001), where $\Delta\Delta$ Ct is the difference between control value (Δ Ct_{co}) and treatment value (Δ Ct_{treated}).

Isotope-Labeling Experiments

For monitoring Suc uptake and partitioning of grains, stems were cut approximately 20 cm below the ear and placed for 6 h in 200 mL of nutrient solution

containing 20 mM KH₂PO₄, 25 mM Suc, 5 mM Gln, 5 mM Asn, 10 mM MES buffer, 1 mM CaCl₂, pH 5.5, and 500 μ L of [U-¹⁴C]-Suc (7.4 MBq mL⁻¹; Amersham-Buchler). During this period, the ears were held under lit (600 μ E) or nonlit conditions. Subsequently, seeds were rapidly removed from the ear and immediately frozen in liquid N₂. A subset of seeds was extracted as in Bligh and Dyer (1959), giving a chloroform-soluble fraction containing the lipids. A second set of seeds was ground and extracted three times with 80% (v/v) ethanol. This soluble phase contained ¹⁴C-Suc as well as ¹⁴C-labeled metabolic intermediates. The remaining pellet was dried and subsequently incubated for 24 h at 30°C in 1.5 mL of 50 mM Tris-HCl (pH 7.4) containing 0.08% (w/v) pronase (Sigma). After centrifugation (5 min and 14,000g), the supernatant was collected, giving the protein fraction. The pellet was washed twice in 1 mL of distilled water. To hydrolyze starch, the remaining insoluble material was incubated with 14 units of amyloglucosidase in 1 mL of 50 mM sodium acetate (pH 4.8) for 24 h at 55°C. After centrifugation (10 min and 14,000g), the supernatant was collected, giving the starch fraction. The residue (cell wall) was resuspended in 1 mL of distilled water. Radioactivity in the different fractions was determined by liquid scintillation counting. Counts were corrected for background and quenching by external standards. By combining the different fractions and relating to the weighted sample, the total label uptake was calculated (given in dpm per mg fresh weight of grain). The partitioning to either lipid, protein, cell wall, or starch is given as percentage of total label. For monitoring Gln uptake of grains, we applied the identical setup but used 30 mM ¹⁵N-labeled Gln (without ¹⁴C-Suc in media; CDN Isotopes). The amount of ^{14/15}N-label was determined in the dry, powdered grain samples using elemental analysis (Vario EL3; Elementaranalysesysteme) coupled to isotope ratio mass spectrometry (ESD 100; IPI).

Supplemental Data

The following supplemental materials are available.

Supplemental Figure S1. Model-predicted flux maps depicting the central metabolic processes occurring in the embryo, endosperm, and pericarp under lit conditions.

Supplemental Figure S2. Model-predicted flux maps depicting the central metabolic processes occurring in the embryo, endosperm, and pericarp under nonlit conditions.

Supplemental Methods S1. Construction and parameterization of the FBA model.

Supplemental Movie S1. Three-dimensional model of the wheat ear derived from MRI data.

Supplemental Movie S2. Three-dimensional model of the barley ear derived from MRI data.

Supplemental Movie S3. Internal structures of the wheat ear in transversal view; data derived from three-dimensional MRI.

Supplemental Movie S4. Internal structures of the barley ear in longitudinal view; data derived from three-dimensional MRI.

Supplemental Data Set S1. Biomass composition, experimental data, biomass equations, and growth rates used for model parameterization.

Supplemental Data Set S2. Set of reactions included in the reconstructed network of barley seed metabolism and the respective references supporting each network reaction.

Supplemental Data Set S3. Model-predicted flux values and ranges.

Supplemental Data Set S4. Complete list of differentially expressed genes from developing grains incubated under lit versus nonlit conditions.

Supplemental Data Set S5. List of primers used in qRT-PCRs.

ACKNOWLEDGMENTS

We thank Katrin Blaschek and Andre Gündel for assistance with enzyme analysis, Mohammad Hajirezaei for help with ¹⁴C isotope studies, Karin Lipfert for artwork, and Nese Sreenivasulu for help with array analysis.

Received July 8, 2015; accepted September 20, 2015; published September 22, 2015.

LITERATURE CITED

- Allen DK, Ohlrogge JB, Shachar-Hill Y (2009) The role of light in soybean seed filling metabolism. *Plant J* **58**: 220–234
- Alonso AP, Goffman FD, Ohlrogge JB, Shachar-Hill Y (2007) Carbon conversion efficiency and central metabolic fluxes in developing sunflower (*Helianthus annuus* L.) embryos. *Plant J* **52**: 296–308
- Alonso AP, Val DL, Shachar-Hill Y (2011) Central metabolic fluxes in the endosperm of developing maize seeds and their implications for metabolic engineering. *Metab Eng* **13**: 96–107
- Amthor JS (2010) From sunlight to phytomass: on the potential efficiency of converting solar radiation to phyto-energy. *New Phytol* **188**: 939–959
- Andriunas FA, Zhang HM, Xia X, Patrick JW, Offler CE (2013) Intersection of transfer cells with phloem biology—broad evolutionary trends, function, and induction. *Front Plant Sci* **4**: 221
- Baghalian K, Hajirezaei MR, Schreiber F (2014) Plant metabolic modeling: achieving new insight into metabolism and metabolic engineering. *Plant Cell* **26**: 3847–3866
- Belmonte MF, Kirkbride RC, Stone SL, Pelletier JM, Bui AQ, Yeung EC, Hashimoto M, Fei J, Harada CM, Munoz MD, et al (2013) Comprehensive developmental profiles of gene activity in regions and subregions of the Arabidopsis seed. *Proc Natl Acad Sci USA* **110**: E435–E444
- Bligh EG, Dyer WJ (1959) A rapid method of total lipid extraction and purification. *Can J Biochem Physiol* **37**: 911–917
- Bolstad BM, Irizarry RA, Astrand M, Speed TP (2003) A comparison of normalization methods for high density oligonucleotide array data based on variance and bias. *Bioinformatics* **19**: 185–193
- Borisjuk L, Neuberger T, Schwender J, Heinzl N, Sunderhaus S, Fuchs J, Hay JO, Tschiersch H, Braun HP, Denolf P, et al (2013) Seed architecture shapes embryo metabolism in oilseed rape. *Plant Cell* **25**: 1625–1640
- Borisjuk L, Nguyen TH, Neuberger T, Rutten T, Tschiersch H, Claus B, Feussner I, Webb AG, Jakob P, Weber H, et al (2005) Gradients of lipid storage, photosynthesis and plastid differentiation in developing soybean seeds. *New Phytol* **167**: 761–776
- Borisjuk L, Rolletschek H, Neuberger T (2012) Surveying the plant's world by magnetic resonance imaging. *Plant J* **70**: 129–146
- Cheung CY, Williams TC, Poolman MG, Fell DA, Ratcliffe RG, Sweetlove LJ (2013) A method for accounting for maintenance costs in flux balance analysis improves the prediction of plant cell metabolic phenotypes under stress conditions. *Plant J* **75**: 1050–1061
- Cheung CYM, Poolman MG, Fell DA, Ratcliffe RG, Sweetlove LJ (2014) A diel flux balance model captures interactions between light and dark metabolism during day-night cycles in *C₃* and Crassulacean acid metabolism leaves. *Plant Physiol* **165**: 917–929
- Chory J (2010) Light signal transduction: an infinite spectrum of possibilities. *Plant J* **61**: 982–991
- Cochrane MP, Duffus CM (1979) Morphology and ultrastructure of immature cereal grains in relation to transport. *Ann Bot (Lond)* **44**: 67–72
- De Block M, Van Lijsebettens M (2011) Energy efficiency and energy homeostasis as genetic and epigenetic components of plant performance and crop productivity. *Curr Opin Plant Biol* **14**: 275–282
- Fisher DB, Cash-Clark CE (2000) Sieve tube unloading and post-phloem transport of fluorescent tracers and proteins injected into sieve tubes via severed aphid stylets. *Plant Physiol* **123**: 125–138
- Gibon Y, Blaessing OE, Hannemann J, Carillo P, Höhne M, Hendriks JHM, Palacios N, Cross J, Selbig J, Stitt M (2004) A Robot-based platform to measure multiple enzyme activities in *Arabidopsis* using a set of cycling assays: comparison of changes of enzyme activities and transcript levels during diurnal cycles and in prolonged darkness. *Plant Cell* **16**: 3304–3325
- Goffman FD, Alonso AP, Schwender J, Shachar-Hill Y, Ohlrogge JB (2005) Light enables a very high efficiency of carbon storage in developing embryos of rapeseed. *Plant Physiol* **138**: 2269–2279
- Gomes de Oliveira Dal'Molin C, Quek LE, Saa PA, Nielsen LK (2015) A multi-tissue genome-scale metabolic modeling framework for the analysis of whole plant systems. *Front Plant Sci* **6**: 4
- Grafahrend-Belau E, Junker A, Eschenröder A, Müller J, Schreiber F, Junker BH (2013) Multiscale metabolic modeling: dynamic flux balance analysis on a whole-plant scale. *Plant Physiol* **163**: 637–647
- Grafahrend-Belau E, Schreiber F, Koschützki D, Junker BH (2009) Flux balance analysis of barley seeds: a computational approach to study systemic properties of central metabolism. *Plant Physiol* **149**: 585–598
- Guichard S, Gary C, Leonardi C, Bertin N (2005) Analysis of growth and water relations of tomato fruits in relation to air vapor pressure deficit and plant fruit load. *J Plant Growth Regul* **24**: 201–213
- Hay J, Schwender J (2011) Computational analysis of storage synthesis in developing *Brassica napus* L. (oilseed rape) embryos: flux variability analysis in relation to ¹³C metabolic flux analysis. *Plant J* **67**: 513–525
- Hay JO, Shi H, Heinzl N, Hebbelmann J, Rolletschek H, Schwender J (2014) Integration of a constraint-based metabolic model of *Brassica napus* developing seeds with ¹³C-metabolic flux analysis. *Front Plant Sci* **5**: 724
- Hueper K, Rong S, Gutberlet M, Hartung D, Mengel M, Lu X, Haller H, Wacker F, Meier M, Gueler F (2013) T2 relaxation time and apparent diffusion coefficient for noninvasive assessment of renal pathology after acute kidney injury in mice: comparison with histopathology. *Invest Radiol* **48**: 834–842
- James MG, Denyer K, Myers AM (2003) Starch synthesis in the cereal endosperm. *Curr Opin Plant Biol* **6**: 215–222
- Jenner CF, Xia Y, Eccles CD, Callaghan PT (1988) Circulation of water within wheat grain revealed by nuclear magnetic resonance micro-imaging. *Nature* **336**: 399–402
- Jonik C, Sonnewald U, Hajirezaei MR, Flügge UI, Ludewig F (2012) Simultaneous boosting of source and sink capacities doubles tuber starch yield of potato plants. *Plant Biotechnol J* **10**: 1088–1098
- Kartäusch R, Helluy X, Jakob PM, Fidler F (2014) Optimization of the AC-gradient method for velocity profile measurement and application to slow flow. *J Magn Reson* **248**: 131–136
- Köckenberger W, De Panfilis C, Santoro D, Dahiya P, Rawsthorne S (2004) High resolution NMR microscopy of plants and fungi. *J Microsc* **214**: 182–189
- Krishnan P, Joshi DK, Maheswari M, Nagarajan S (2004) Characterisation of soybean and wheat seeds by nuclear magnetic resonance spectroscopy. *Biol Plant* **48**: 117–120
- Krishnan P, Singh R, Verma APS, Joshi DK, Singh S (2014) Changes in seed water status as characterized by NMR in developing soybean seed grown under moisture stress conditions. *Biochem Biophys Res Commun* **444**: 485–490
- Lau OS, Deng XW (2010) Plant hormone signaling lightens up: integrators of light and hormones. *Curr Opin Plant Biol* **13**: 571–577
- Livak KJ, Schmittgen TD (2001) Analysis of relative gene expression data using real-time quantitative PCR and the 2^{-ΔΔCT} method. *Methods* **25**: 402–408
- Mahadevan R, Schilling CH (2003) The effects of alternate optimal solutions in constraint-based genome-scale metabolic models. *Metab Eng* **5**: 264–276
- Mangelsen E, Wanke D, Kilian J, Sundberg E, Harter K, Jansson C (2010) Significance of light, sugar, and amino acid supply for diurnal gene regulation in developing barley caryopses. *Plant Physiol* **153**: 14–33
- Matsuhashi S, Fujimaki S, Uchida H, Ishioka NS, Kume T (2006) A new visualization technique for the study of the accumulation of photo-assimilates in wheat grains using [¹¹C]CO₂. *Appl Radiat Isot* **64**: 435–440
- Melkus G, Rolletschek H, Fuchs J, Radchuk V, Grafahrend-Belau E, Sreenivasulu N, Rutten T, Weier D, Heinzl N, Schreiber F, et al (2011) Dynamic ¹³C/¹H NMR imaging uncovers sugar allocation in the living seed. *Plant Biotechnol J* **9**: 1022–1037
- Metzner R, van Dusschoten D, Bühler J, Schurr U, Jahnke S (2014) Belowground plant development measured with magnetic resonance imaging (MRI): exploiting the potential for non-invasive trait quantification using sugar beet as a proxy. *Front Plant Sci* **5**: 469
- Michalska J, Zauber H, Buchanan BB, Cejudo FJ, Geigenberger P (2009) NTRC links built-in thioredoxin to light and sucrose in regulating starch synthesis in chloroplasts and amyloplasts. *Proc Natl Acad Sci USA* **106**: 9908–9913
- Mintz-Oron S, Meir S, Malitsky S, Ruppin E, Aharoni A, Shlomi T (2012) Reconstruction of Arabidopsis metabolic network models accounting for subcellular compartmentalization and tissue-specificity. *Proc Natl Acad Sci USA* **109**: 339–344
- Neuberger T, Sreenivasulu N, Rokitta M, Rolletschek H, Göbel C, Rutten T, Radchuk V, Feussner I, Wobus U, Jakob P, et al (2008) Quantitative imaging of oil storage in developing crop seeds. *Plant Biotechnol J* **6**: 31–45
- Peukert M, Thiel J, Peshev D, Weschke W, Van den Ende W, Mock HP, Matros A (2014) Spatio-temporal dynamics of fructan metabolism in developing barley grains. *Plant Cell* **26**: 3728–3744

- Poolman MG, Miguet L, Sweetlove LJ, Fell DA (2009) A genome-scale metabolic model of *Arabidopsis* and some of its properties. *Plant Physiol* **151**: 1570–1581
- Prado K, Boursiac Y, Tournaire-Roux C, Monneuse JM, Postaire O, Da Ines O, Schäffner AR, Hem S, Santoni V, Maurel C (2013) Regulation of *Arabidopsis* leaf hydraulics involves light-dependent phosphorylation of aquaporins in veins. *Plant Cell* **25**: 1029–1039
- Radchuk V, Borisjuk L (2014) Physical, metabolic and developmental functions of the seed coat. *Front Plant Sci* **5**: 510
- Radchuk V, Weier D, Radchuk R, Weschke W, Weber H (2011) Development of maternal seed tissue in barley is mediated by regulated cell expansion and cell disintegration and coordinated with endosperm growth. *J Exp Bot* **62**: 1217–1227
- Radchuk VV, Borisjuk L, Sreenivasulu N, Merx K, Mock HP, Rolletschek H, Wobus U, Weschke W (2009) Spatiotemporal profiling of starch biosynthesis and degradation in the developing barley grain. *Plant Physiol* **150**: 190–204
- Rahmani F, Hummel M, Schuurmans J, Wiese-Klinkenberg A, Smeekens S, Hanson J (2009) Sucrose control of translation mediated by an upstream open reading frame-encoded peptide. *Plant Physiol* **150**: 1356–1367
- Rolletschek H, Koch K, Wobus U, Borisjuk L (2005) Positional cues for the starch/lipid balance in maize kernels and resource partitioning to the embryo. *Plant J* **42**: 69–83
- Rolletschek H, Melkus G, Grafahrend-Belau E, Fuchs J, Heinzl N, Schreiber F, Jakob PM, Borisjuk L (2011) Combined noninvasive imaging and modeling approaches reveal metabolic compartmentation in the barley endosperm. *Plant Cell* **23**: 3041–3054
- Rolletschek H, Weschke W, Weber H, Wobus U, Borisjuk L (2004) Energy state and its control on seed development: Starch accumulation is associated with high ATP and steep oxygen gradients within barley grains. *J Exp Bot* **55**: 1351–1359
- Rontein D, Dieuaide-Noubhani M, Dufourc EJ, Raymond P, Rolin D (2002) The metabolic architecture of plant cells. Stability of central metabolism and flexibility of anabolic pathways during the growth cycle of tomato cells. *J Biol Chem* **277**: 43948–43960
- Sairanen I, Novák O, Pěncík A, Ikeda Y, Jones B, Sandberg G, Ljung K (2012) Soluble carbohydrates regulate auxin biosynthesis via PIF proteins in *Arabidopsis*. *Plant Cell* **24**: 4907–4916
- Sanchez-Bragado R, Molero G, Reynolds MP, Araus JL (2014) Relative contribution of shoot and ear photosynthesis to grain filling in wheat under good agronomical conditions assessed by differential organ $\delta^{13}\text{C}$. *J Exp Bot* **65**: 5401–5413
- Schiebold S, Tschiersch H, Borisjuk L, Heinzl N, Radchuk R, Rolletschek H (2011) A novel procedure for the quantitative analysis of metabolites, storage products and transcripts of laser microdissected seed tissues of *Brassica napus*. *Plant Methods* **7**: 19
- Schwender J, Hebbelmann I, Heinzl N, Hildebrandt T, Rogers A, Naik D, Klapperstück M, Braun HP, Schreiber F, Denolf P, et al (2015). Quantitative multilevel analysis of central metabolism in developing oilseeds of oilseed rape during in vitro culture. *Plant Physiol* **168**: 828–848
- Schwender J, König C, Klapperstück M, Heinzl N, Munz E, Hebbelmann I, Hay JO, Denolf P, De Bodt S, Redestig H, et al (2014) Transcript abundance on its own cannot be used to infer fluxes in central metabolism. *Front Plant Sci* **5**: 668
- Skillman JB (2008) Quantum yield variation across the three pathways of photosynthesis: not yet out of the dark. *J Exp Bot* **59**: 1647–1661
- Smeekens S, Ma J, Hanson J, Rolland F (2010) Sugar signals and molecular networks controlling plant growth. *Curr Opin Plant Biol* **13**: 274–279
- Sreenivasulu N, Radchuk V, Strickert M, Miersch O, Weschke W, Wobus U (2006) Gene expression patterns reveal tissue-specific signaling networks controlling programmed cell death and ABA-regulated maturation in developing barley seeds. *Plant J* **47**: 310–327
- Sweetlove LJ, Beard KFM, Nunes-Nesi A, Fernie AR, Ratcliffe RG (2010) Not just a circle: flux modes in the plant TCA cycle. *Trends Plant Sci* **15**: 462–470
- Sweetlove LJ, Obata T, Fernie AR (2014) Systems analysis of metabolic phenotypes: What have we learnt? *Trends Plant Sci* **19**: 222–230
- Sweetlove LJ, Ratcliffe RG (2011) Flux-balance modeling of plant metabolism. *Front Plant Sci* **2**: 38
- Tiessen A, Nerlich A, Faix B, Hümmer C, Fox S, Trafford K, Weber H, Weschke W, Geigenberger P (2012) Subcellular analysis of starch metabolism in developing barley seeds using a non-aqueous fractionation method. *J Exp Bot* **63**: 2071–2087
- Tran V, Weier D, Radchuk R, Thiel J, Radchuk V (2014) Caspase-like activities accompany programmed cell death events in developing barley grains. *PLoS One* **9**: e109426
- Tschiersch H, Borisjuk L, Rutten T, Rolletschek H (2011) Gradients of seed photosynthesis and its role for oxygen balancing. *Biosystems* **103**: 302–308
- Tschiersch H, Liebsch G, Borisjuk L, Stangelmayer A, Rolletschek H (2012) An imaging method for oxygen distribution, respiration and photosynthesis at a microscopic level of resolution. *New Phytol* **196**: 926–936
- Udvardi MK, Czechowski T, Scheible WR (2008) Eleven golden rules of quantitative RT-PCR. *Plant Cell* **20**: 1736–1737
- Van As H (2007) Intact plant MRI for the study of cell water relations, membrane permeability, cell-to-cell and long distance water transport. *J Exp Bot* **58**: 743–756
- Van As H, Scheenen T, Vergeldt FJ (2009) MRI of intact plants. *Photosynth Res* **102**: 213–222
- Van As H, van Duynhoven J (2013) MRI of plants and foods. *J Magn Reson* **229**: 25–34
- van Bel AJ, Helariutta Y, Thompson GA, Ton J, Dinant S, Ding B, Patrick JW (2013) Phloem: the integrative avenue for resource distribution, signaling, and defense. *Front Plant Sci* **4**: 471
- Van Der Weerd L, Claessens MMAE, Efde C, Van As H (2002) Nuclear magnetic resonance imaging of membrane permeability changes in plants during osmotic stress. *Plant Cell Environ* **25**: 1539–1549
- Walton JH, Conradi MS (1987) Flow velocity measurement with ac gradients. *Magn Reson Med* **4**: 274–281
- Williams TCR, Miguet L, Masakapalli SK, Kruger NJ, Sweetlove LJ, Ratcliffe RG (2008) Metabolic network fluxes in heterotrophic *Arabidopsis* cells: stability of the flux distribution under different oxygenation conditions. *Plant Physiol* **148**: 704–718
- Wu Y, Yang R, Jia S, Li Z, Zhou Z, Lou T (2014) Computer-aided diagnosis of early knee osteoarthritis based on MRI T2 mapping. *Biomed Mater Eng* **24**: 3379–3388